中國機械工程學刊第四十二卷第三期第 285~294 頁(民國一百一十年)
Journal of the Chinese Society of Mechanical Engineers, Vol.42, No.3, pp 285~294 (2021)

Thermal Contact Resistance Model of Annular Contact Surfaces with Various Tolerance Fits for Spindle-Bearing Joint

Cui Fang*, Cong-Bin Yang***, Qiu-shi Hu**, Yong-Sheng Zhao*** and Zhi-Feng Liu***

Keywords: spindle-bearing joint, thermal contact resistance, tolerance fit, contact load, fractal theory.

ABSTRACT

The thermal contact resistance (TCR) of a spindle-bearing joint is crucial in the analysis of thermal characteristics of high speed motorized spindle, which could severely affect the machining accuracy of a machine tool. In this research, firstly, an experimental set-up was designed and the one-dimensional steady measurement method was introduced to obtain the TCR of an annular contact surface with various tolerance fits. Secondly, a TCR model of an annular contact surface for the spindle-bearing joint with various tolerance fits was proposed. The TCR model was obtained by the constrained thermal resistance, the bulk thermal resistance and the air thermal resistance. Finally, the clearance, transition and interference fits were considered as three typical cases. The TCR of the interference fit could be calculated based on the proposed model and the contact load derived from the contact formula. However, this method was not suitable for the cases of clearance and transition fits. In this case, a hybrid method was utilized to determine the corresponding equivalent contact load. The results demonstrated that the proposed model could be utilized to predict the TCR of annular surfaces with various tolerance fits.

INTRODUCTION

The thermal error of the high speed motorized spindle constitutes one of the most significant sources of the CNC machining center inaccuracy. Although the thermal error can be reduced through compensation techniques, it cannot be fully eliminated in a real machining environment due to technical limitations. The thermal error of the high-speed motorized spindle constitutes one of the most significant sources of the CNC machining center inaccuracy. Although the thermal error can be reduced through compensation techniques, it cannot be fully eliminated in a real machining environment due to technical limitations. Moreover, the excessive temperature increase would limit the speed improvement for the high-speed motorized spindle, resulting in reduced processing efficiency. An accurate thermal characteristic model is vital for the thermal error optimization or prediction of the high-speed motorized spindle. In contrast, the thermal contact resistance (TCR) commonly exists in the high-speed motorized spindle, which can affect the temperature distribution and deformation of the spindle. In particular, the TCR of the spindle-bearing joint is the most important for the high-speed motorized spindle, which can directly affect the heat transfer and lead to temperature increase of the bearing. It is therefore necessary to model the TCR of spindle-bearing joint with various tolerance fits.

The TCR of contact surfaces can be obtained based on experimental methods. Zhang *et al* proposed a device for the TCR measurement of the interface based on a reversible heat flow method. Zain *et al* investigated the effect of interfacial thermal resistance (TR) on the effective thermal conductivity of Cu/D composites through experimental and numerical methods. Zheng *et al* introduced an improved thermal contact resistance (TCR) model, which matched well with the experimental data for the pressed stainless steel 304. The solid/liquid contact resistance was also obtained using the ideal gas law by assuming trapped air in the micro gaps. Ahadi *et al* proposed a new modified TPS method, which allowed an accurate measurement of the bulk thermal conductivity of thin films and coatings. Zhang *et al* investigated the TCR of five types of aluminum alloy materials through experimental measurement and detailed analysis. The relationship among TCR, pressure and temperature was determined.

Although the TCR of contact surfaces can be obtained using experimental methods, it is difficult to describe the relationship between TCR and the

Paper Received July, 2020. Revised Sepfember, 2020. Accepted October, 2020. Author for Correspondence: Yong-Sheng Zhao

* *Ph.D. student, Institute of Advanced Manufacturing and Intelligent Technology, Beijing University of Technology, Beijing 100124, China.*

** *Lecturer, School of Mechanical Engineering, Jiangsu University of Science and Technology, Zhenjiang 212003, China.*

*** *Professor, Institute of Advanced Manufacturing and Intelligent Technology, Beijing University of Technology, Beijing 100124,China.*

corresponding influencing factors, such as contact load, surface topology and materials. For the contact surfaces, the fractal theory can be utilized to describe the micro-contact of the asperities. Majumdar first presented the fractal theory to describe the surface topography. Later, Majumdar and Bhushan established the famous M-B fractal contact model. According to this model, the rough surface could be characterized by the fractal dimension D and the fractal roughness parameter G. The fractal parameters were independent and not affected by the instrument resolution. A large number of researchers further developed the M-B model, and focused on the fractal topography characterization, the elastic-plastic mechanics and the contact areas. The fractal contact theory provides an effective way to study the TCC of contact surfaces. Xu *et al* developed the model of TCR based on the fractal contact theory. The classic heat transfer theory and the improved M-B fractal contact model were introduced to obtain the TCR. Zou *et al* developed a random model based on the fractal geometry theory, which considered both the microscopic bulk resistance and the constriction resistance to calculate the TCR between two rough surfaces with elastic and fully plastic deformation. Chen *et al* developed a model of laminar heat transfer in rough micro channels, based on the topography of rough surfaces characterized through a Cantor fractal structure. Ji *et al* established the fractal prediction model of the TCC based on the three-dimensional fractal model. Jiang *et al* proposed an analytical model of thermal contact resistance based on the Weierstrass-Mandelbrot fractal function. Fang *et al* developed a patching type multi-block lattice Boltzmann method to predict the TCR at the interface of two solids. Ma *et al* introduced the comprehensive geometrical–mechanical–thermal predictive model for thermal contact conductance between two flat metallic rough surfaces. Surya Kumar presented steady state thermal contact conductance analysis on two solid bodies of brass, with flat and curvilinear contact combinations, under variable loading conditions ranging between 0.27 and 4.0 kN. Vladislav A introduced a corrective function to compensate errors in contact area computations using mesh discretization based on geometrical arguments. Wang *et al* carried out a detailed examination of the related characteristics of a gas bearing shaft system using numerical value analysis such as the finite difference and differential transformation methods. Wang *et al* explored the related characteristics for spindle system with the finite difference method and mixed method to prevent irregular vibration and reduce instantaneous air hammer effect. The TCR can be obtained for flat contact surfaces by using the aforementioned experimental or theoretical methods. In contrast, these methods are not applicable for the annular contact surfaces of the spindle-bearing joint, as it is difficult to determine the contact state for the TCR acquisition with various tolerance fits.

The main objective of this study was to model the TCR of annular surfaces for the spindle-bearing joint based on the fractal theory. It was assumed that the rough contact surface was composed of numerous, discrete and parallel micro-contact cylinders. The TCR can be calculated by integrating the micro asperities, where the constrained thermal resistance of micro-contacts, the bulk thermal resistance of micro asperities and air medium thermal resistance of the micro gap were considered. An experimental set-up was designed and the one-dimensional steady measurement method was introduced to obtain the TCR of the annular contact surface with various tolerance fits. For the interference fit, the theoretical and experimental results were compared and the proposed model was verified. For the transition and clearance fits, a hybrid method was utilized to determine the corresponding equivalent contact load based on the experimental and theoretical results. This study would provide a theoretical basis for analysis or optimization of the thermal characteristics of the high-speed motorized spindle.

TCR EXPERIMENTAL SET-UP OF ANNULAR CONTACT SURFACES

The schematic diagram of the high speed motorized spindle is presented in Fig. 1, where the heat originated from the stator and rotor of the motor, along with the front and the rear bearing. In order to suppress the increase in temperature of the spindle system, the cooling system was placed on the motor and the bearing corresponding to the spindle housing. In contrast, the heat transfer of the spindle system could be affected by the annular contact surfaces of the spindle-bearing joint. Usually, three tolerance fits (interference fit, transition fit and clearance fit) are utilized to support the spindle shaft. In this paper, an experimental set-up was designed to obtain the thermal contact resistance of the annular contact surfaces with various tolerance fits. The schematic diagram of the experimental set-up is presented in Fig. 2. To ensure the heat flow radial spread, a heating device was arranged in the middle of the entire device and a cooling device was placed outside the outer testing piece. The heat insulating material was aerogel thermal blanket, which filled the upper and lower parts of the testing pieces. Shielding was utilized to form the vacuum confined space for air thermal convection effect reduction. The PT100 type temperature sensors were arranged on the same plane to reduce the measurement error. The term $R_{i,j}$ represents the distribution radii of the temperature sensors, where the subscript $i = 1,2,3$ indicates the calibrated copper ring, the inner test specimen and the outer test specimen. The subscript $j = 1,2$ indicates the number of temperature sensors in each testing piece. The term R_x is the radius of the annular contact surface. To ensure good thermal conductivity, the thermal grease was spread between the heat flow meter of the calibrated copper ring and the inner test specimen. The experimental set-up and the test specimen are presented in Figs.3 and 4. The test specimen was turned and then ground. The surface roughness was 1.6 μm. The parameters of the test specimen and the radial distribution of all temperature sensors are illustrated in Table 1, where the inner radius of the outer test specimen was equal to the outer radius of the inner test specimen as

$R_{oi} = R_{io}$. For the paired test specimens, the interference, the transition and the clearance fits were respectively manufactured for the effect of tolerance fit on the thermal contact resistance to be obtained.

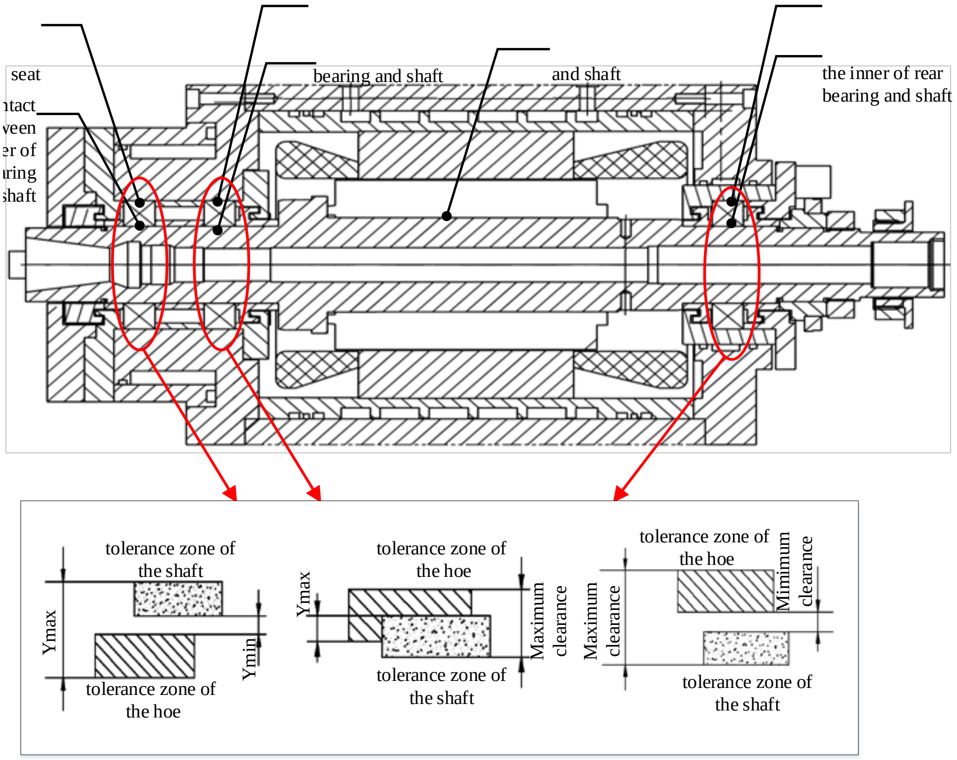

Fig. 1. Schematic diagram of high speed motorized spindle

Table 1 Parameters of test piece

Dimension parameters of test pieces (mm)				Radius of temperature sensors (mm)						
Outer radius of outer test piece R_{oo}	Inner radius of outer test piece R_{oi}	Inner radius of inner test piece R_{ii}	Length of contact surface L_T	R_{11}	R_{12}	R_{21}	R_{22}	R_{31}	R_{32}	R_x
60	40	20	100	10	15	25	35	45	55	40

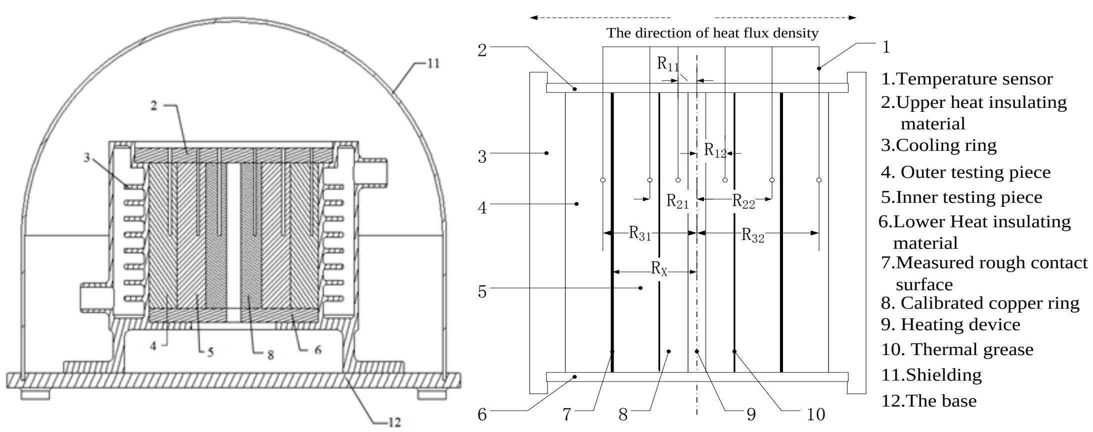

Fig. 2. Schematic diagram of experimental set-up

Fig. 3. Experimental set-up

Fig. 4. Test specimen

The entire device was heated by a heating device of 300W. The temperature of each measurement point $T_{i,j}$ in the location of $R_{i,j}$ was recorded until the temperature change was below 0.5℃ within 20 minutes. The gradient distribution of the measured temperatures is presented in Fig.5. The one-dimensional steady measurement method was introduced to obtain the TCC of the annular interface, where the radial steady gradient of the heat flow in one-dimension for the test pieces could be directly measured. The temperature difference of the contact surface can be given as:

$$\Delta T = T_{21} - \frac{T_{21}-T_{22}}{ln(\frac{R_{21}}{R_{22}})} ln(\frac{R_X}{R_{21}}) - [T_{31} - \frac{T_{31}-T_{32}}{ln(\frac{R_{31}}{R_{32}})} ln(\frac{R_X}{R_{31}})] \quad (1)$$

As the thermal conductivity of the calibrated copper ring was $\lambda_{copper} = 397w/km$, the heat flux of the contact interface was calculated as: $R_{Cg}=2.93 \times 10^{-4}(°c \cdot m^2)/W$

$$q_{R_X} = \frac{\lambda_{copper}\frac{T_{11}-T_{12}}{ln\frac{R_{12}}{R_{11}}}}{R_X} \quad (2)$$

By combining Eqs. (1) and (2), the TCR can be given as:

$$R^* = \frac{\Delta T}{q_{R_X}} \quad (3)$$

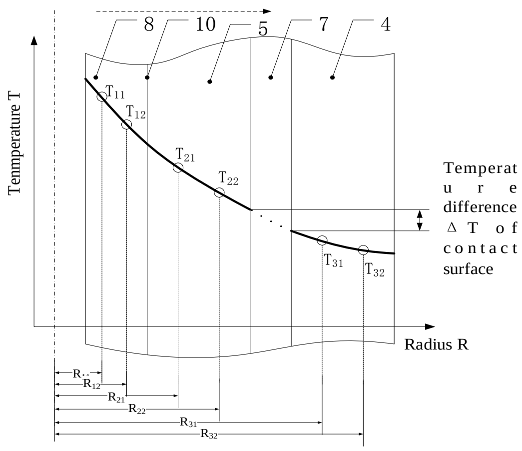

Fig. 5. Gradient distribution of temperature

TCR model of annular contact surfaces based on fractal theory

The TCR prediction model of the annular contact surfaces is crucial for the optimization or analysis of thermal characteristics of the high-speed motorized spindle. For the machined annular contact surfaces, the fractal theory could be introduced to describe the surface topology. The two rough annular surfaces could be simplified by a perfectly smooth plane and an equivalent fractal rough surface. The asperities from one solid were squeezed against the asperities from another solid, when two rough surfaces were brought in contact, which led the asperities to deform elastically or plastically. According to the Hertz contact theory, the contact load for one micro-contact is defined as:

$$\begin{cases} f_e = \frac{2^{\frac{9-2D}{2}}E}{3\pi^{\frac{3-D}{2}}}(ln\,\gamma)^{\frac{1}{2}}G^{D-1}a'^{\frac{3-D}{2}} & \text{Elastic deformation} \\ f_p = K\sigma_y a' & \text{Plastic defromation} \end{cases} \quad (4)$$

where, Drepresents the fractal dimension, $G$is the fractal roughness parameter, γ controls the frequency density

of the surface roughness and $\gamma = 1.5$, E is the equivalent elastic modulus of the two contact materials $E = \left(\frac{(1-\nu_1^2)}{E_1 + \frac{(1-\nu_2^2)}{E_2}}\right)^{-1}$, ν_1, ν_2, E_1, E_2 are the Poisson ratios and elastic moduli of the two in contact materials, respectively. K is the coefficient of hardness $K = 2.8$, σ_y is the yield strength of softer materials, a' is truncated area of a micro-contact.
The statistical distribution of the truncated area a' of the micro-contact can be described as

$$n(a') = \frac{D}{2}\Psi^{\frac{(2-D)}{2}} {a'_L}^{\frac{D}{2}} {a'}^{-\frac{D+2}{2}} \tag{5}$$

where, a'_L is the truncated area of the largest elastic micro-contact, Ψ describes the domain extension factor for the micro-contact size distribution and is given by the following equation

$$\left(\Psi^{\frac{(2-D)}{2}} - \left(1 + \Psi^{\frac{(-D)}{2}}\right)^{\frac{-(2-D)}{D}}\right) / \left((2-D)/D\right) = 1.$$

The total normal load and real contact area can be obtained by integrating the micro asperities, given as:

$$\begin{aligned} F &= \int_0^{a'_c} f_p n(a')\, da' + \int_{a'_c}^{a'_L} f_e\, n(a') da' \\ &= K\sigma_y \frac{D}{2-D} \Psi^{\frac{(2-D)}{2}} {a'_L}^{\frac{D}{2}} {a'_c}^{\frac{2-D}{2}} + \frac{2^{\frac{9-2D}{2}}}{3\pi^{\frac{3-D}{2}}} \frac{D}{3-2D} (\ln\gamma)^{\frac{1}{2}} G^{D-1} E \Psi^{\frac{(2-D)}{2}} {a'_L}^{\frac{D}{2}} \left({a'_L}^{\frac{3-2D}{2}} - {a'_c}^{\frac{3-2D}{2}}\right) \quad D \neq 1.5 \end{aligned} \tag{6}$$

$$\begin{aligned} F &= \int_0^{a'_c} f_p n(a')\, da' + \int_{a'_c}^{a'_L} f_e\, n(a') da' \\ &= 3K\sigma_y \Psi^{\frac{1}{4}} {a'_L}^{\frac{3}{4}} {a'_c}^{\frac{1}{4}} + \frac{2}{\pi^{\frac{3}{4}}} (\ln\gamma)^{\frac{1}{2}} G^{\frac{1}{2}} E \Psi^{\frac{1}{4}} {a'_L}^{\frac{3}{4}} \left(\ln\frac{a'_L}{a'_c}\right) \quad D = 1.5 \end{aligned} \tag{7}$$

$$A_r = \int_0^{a'_c} n(a')\, a' da' + \int_{a'_c}^{a'_L} n(a') \frac{1}{2} a' da' = \frac{D}{4-2D} \Psi^{\frac{(2-D)}{2}} {a'_L}^{\frac{D}{2}} {a'_c}^{\frac{2-D}{2}} + \frac{D}{4-2D} \Psi^{\frac{(2-D)}{2}} a'_L \tag{8}$$

where, a'_c is the critical area from the elastic deformation to the plastic deformation and can be defined as:

$$a'_c = \left[2^{(9-2D)} \pi^{(D-3)} (0.454 + 0.41\nu_1)^{(-2)} G^{(2D-2)} \left(\frac{E}{K\sigma_y}\right)^2 \ln\gamma\right]^{\frac{1}{D-1}} \tag{9}$$

The heat flow under steady state conditions across the joints was constrained through the individual micro-contacts. As shown in Fig.6, the thermal contact resistance (TCR) was composed of the constrained resistance R_c, the bulk thermal resistance R_b and the gap thermal resistance R_g.

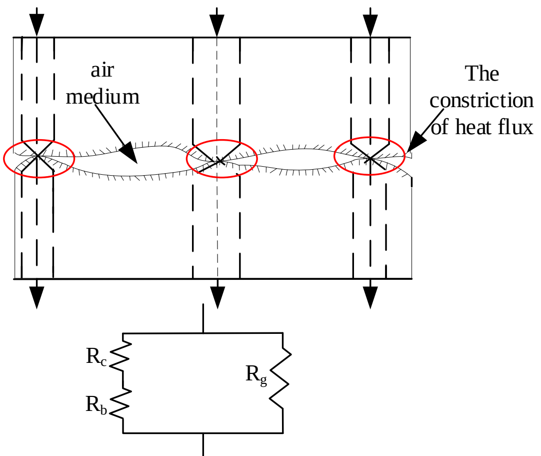

Fig. 6. The micro surface morphology of joint and thermal contact resistance

For the low-sized heat channels, the following assumptions were made: (1) No heat exchange between heat flow channels; (2) The temperature differences of all heat channel interfaces were similar; (3) Heat transfer through the gap was full of air. Only the heat conductivity was considered, whereas the heat radiation and heat convection were ignored for the presented model. The TCR can be expressed as:

$$\frac{1}{R} = \frac{1}{R_b + R_c} + \frac{1}{R_g} = \frac{1}{R_{bc}} + \frac{1}{R_g} \tag{10}$$

The bulk thermal resistance can be expressed as:

$$r_b = \frac{2d'}{ka'} \tag{11}$$

where, k is the equivalent heat conduction coefficient $k = k_1 \cdot k_2/(k_1 + k_2)$, and k_1, k_2 are the thermal conductivity coefficients of the two contact materials, respectively. d' is the contact height of the micro-contact and $d' = Z'_{max} - \delta_{max}$, Z'_{max} is the distance from the highest point to the lowest point of the sample rough surface which can be simulated by the Weierstrass-Mandelbort (W-M) function $Z'_{max} = L(G/L)^{D-1}$, L is the sample length, and δ_{max} is the maximum deformation of an asperity. $\delta_{max} = G^{D-1} {a'}_L^{\frac{2-D}{2}}$

The constrained thermal resistance of a single micro-contact is given:

$$r_c = \frac{\psi(c/b)}{2kc} = \frac{\sqrt{2\pi}[1-(c/b)]^{3/2}}{2k\sqrt{a'}} = \frac{\sqrt{2\pi}[1-(A_r^*)^{1/2}]^{3/2^{\frac{3}{2}}}}{2k\sqrt{a'}} \tag{12}$$

where, c is the contact radius of the micro-contact and $a' = 2\pi c^2$, b is the radius of the heat flow channel, $c/b = (A_r/A_a)^{1/2} = (A_r^*)^{1/2}$, A_a is the nominal contact area, and $\psi(c/b)$ is the interface constriction coefficient, $\psi(c/b) \approx (1-c/b)^{3/2}$

The bulk and constrained thermal resistance can be given as:

$$r_{bc} = r_b + r_c = \frac{2d'}{ka'} + \frac{\sqrt{2\pi}}{2k\sqrt{a'}}[1-\left(\frac{A_r}{A}\right)^{\frac{1}{2}}]^{\frac{3}{2}} \tag{13}$$

The bulk and constrained thermal resistance of an asperity r_{bce} and r_{bcp} at the elastic and fully plastic deformation can be expressed as:

$$\begin{cases} r_{bce} = \frac{2d'}{ka'} + \frac{\sqrt{2\pi}}{2k\sqrt{a'}}(1-\left(\frac{A_r}{A}\right)^{\frac{1}{2}})^{\frac{3}{2}} \\ r_{bcp} = \frac{d'}{ka'} + \frac{\sqrt{\pi}}{2k\sqrt{a'}}(1-\left(\frac{A_r}{A}\right)^{\frac{1}{2}})^{\frac{3}{2}} \end{cases} \tag{14}$$

The bulk and constrained thermal resistance of annular contact surfaces can be obtained by integrating the asperities of the annular contact surfaces. The bulk and constrained thermal resistance R_{bc} for the annular contact surfaces can be given as:

$$R_{bc} = \int_0^{a_c'} r_{bcp} n(a')\,da' + \int_{a'_c}^{a'_L} r_{bce} n(a')\,da' \tag{15}$$

According to the Maxwell theory for interfacial temperature discontinuity, when the collisions of gas molecules make important contributions to the heat transfer between the plates, a dimensionless discriminant parameter, known as the Knudsen number $0.01 < k_n < 10$ is utilized, whereas the air thermal resistance of the micro gap medium can be defined as:

$$R_g = \frac{M+d}{k_g} \tag{16}$$

where, $k_g = 0.026W/(m \cdot \square)$ is the coefficient of air heat conductivity in the gap with the normal temperature, d is the average gap height of the contact plane, $d = 1.53\sigma\left(\frac{p}{H}\right)^{-0.097}$, σ is the equivalent RMS roughness, $\sigma = \sqrt{\sigma_1^2 + \sigma_1^2}$, σ_1 and σ_2 represent the roughness of the two contact surfaces respectively, H is the hardness of the softer material. According to Ref [24], $M = 2\Lambda\gamma((2-\alpha_1)/\alpha_1 + (2-\alpha_2)/\alpha_2)/(p_r(1+\gamma))$, $\gamma = 1.4$ is the specific heat ratio of gas with the normal temperature, $p_r = 0.69$ is the gas Prandt1 number, α_1 and α_2 are thermal accommodation coefficients corresponding to the two gas/plate interfaces,

$$\alpha = exp[-0.57(\frac{T_s - T_0}{T_0})](\frac{M_g^*}{6.8 + M_g^*}) + \frac{2.4\mu}{(1+\mu)^2}$$
$$\{1 - exp[-0.57(\frac{T_s - T_0}{T_0})]\}$$

$$M_g^* = \begin{cases} M_g & \text{for monatomic gases} \\ 1.4M_g & \text{for diatomic/polyatomic gases} \end{cases}$$

$\mu = M_g/M_s$,M_g and M_s are the molecular weights of the gas and the solid, T_0 is the reference temperature, $T_0 = -0.15°C$, and T_S is the ambient temperature, $T_s = 21.85°C$.

Results and discussion

Verification of the annular surfaces with interference fit

The contact load is necessary for the proposed model to predict the annular contact surfaces TCR of the spindle-bearing joint. For the interference fit of annular surfaces, the inner test specimen was compressed and the outer test specimen was expanded due to the effect of contact pressure, as presented in Fig. 7. The magnitude of interference was the key factor for the contact pressure improvement. The effective magnitude of interference can be defined as:

$$\Delta = \frac{2R_{oi}}{2R_{oi}+3}\Delta_d \tag{17}$$

where, Δ_d is the nominal magnitude of the interference fit.

The displacement of the test specimen can be respectively expressed as:

$$u_o(r) = \frac{R_{oi}^2 p}{E_1(R_{oo}^2 - R_{oi}^2)}\left[(1-v_1)r + \frac{(1+v_1)R_{oo}^2}{r}\right] \tag{18}$$

$$u_i(r) = -\frac{R_{oi}^2 p}{E_2(R_{oo}^2 - R_{oi}^2)}\left[(1-v_2)r + \frac{(1+v_2)R_{ii}^2}{r}\right] \tag{19}$$

where, $u_o(r)$, $u_i(r)$ are the displacements of the outer and inner test specimens, $R_{ii} \le r \le R_{oo}$ is the radius.

The effective magnitude of interference Δ can also be written as:

$$\Delta = 2[u_o(r = R_{oi}) - u_i(r = R_{io})] \tag{20}$$

By substituting Eq. (19) into Eq. (20), the contact stress can be given as:

$$P = \frac{\Delta}{2\left[R_{oi}\frac{(1-v_1)R_{oi}^2 + (1+v_1)R_{oo}^2}{E_1\left(R_{oo}^2 - R_{oi}^2\right)} + R_{io}\frac{(1-v_2)R_{io}^2 + (1+v_2)R_{ii}^2}{E_2\left(R_{io}^2 - R_{ii}^2\right)}\right]} \tag{21}$$

The normal contact load for the interference fit can be expressed as:

$$F_I = PA \tag{22}$$

where, F_I is the contact load of the annular contact surfaces with interference fits, and A denotes the normal contact surface

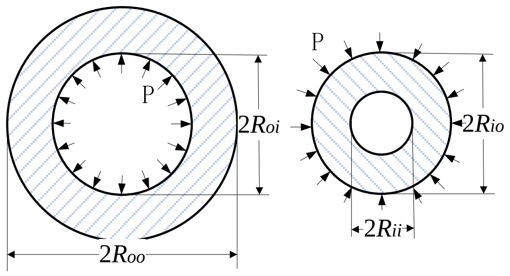

Fig. 7. Contact pressure of annular surfaces with interference fits

The material of the test specimen was stainless steel (12CrNi3A type in China). The elastic modulus, hardness, Poisson ratio and density of the two test pieces were $E_1 = E_2 = 1.9 \times 10^5\,\mathrm{MPa}$, $H_1 = H_2 = 3.8 \times 10^3\,\mathrm{MPa}$, $\nu_1 = \nu_2 = 0.27$, and $\rho_1 = \rho_2 = 7800\frac{kg}{m^3}$, respectively. The thermal conductivity coefficient of the test specimen was $k_{t1} = k_{t2} = 16.2\,\mathrm{W}/(m \cdot °C)$, respectively. The contact surface profile of the test specimen could be measured by a 3-D profilometer, based on the power spectrum density method. The fractal dimension and fractal roughness parameter of contact surface could be obtained as $D = 1.35$ and $G = 1.0 \times 10^{-11}m$. The interference fit of the test specimen was $\Phi 80H6/s5$, where the nominal magnitude of the interference fit was $\Delta_d = 0.03mm$. The temperature was measured every five minutes. The experimental process was repeated four times to reduce the measurement and random errors. The radial distribution of the measured temperature is presented in Fig. 8.

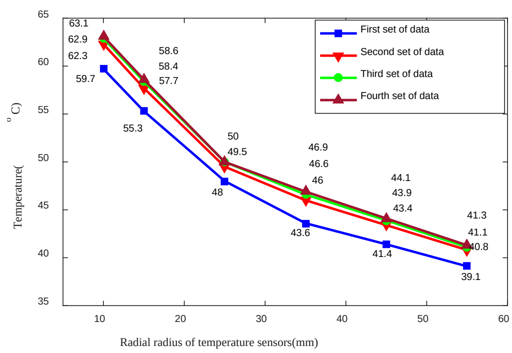

Fig. 8. Measured data of annular surfaces with interference fits

By adding the average temperature from Fig. 8 into Eqs. (1), (2) and (3), the TCR of the annular contact surface in the interference fit could be obtained as $R_I^* = 6.18 \times 10^{-5}(°c \cdot m^2)/\mathrm{W}$. By considering the material characteristic parameters of the test piece from Table 1 in Eqs. (17), (18), (19), (20), (21) and (22), the effective magnitude of interference was obtained as $\Delta = 29\mu m$, the contact stress was obtained as $p = 16Mpa$ and the normal load was obtained as $F_I = 4.0 \times 10^5 N$. The relationships of the total TCR, the bulk and constrained resistance, the gap thermal resistance and the contact load with material of 12CrNi3A at $G = 1.0 \times 10^{-11}m$ and $D = 1.35$ are illustrated in Fig.9. It could be observed that the TCR was provided by the bulk and constrained resistance along with the gap thermal resistance, where the TCR could be obtained as R_I=$5.57 \times 10^{-5}(°c \cdot m^2)/\mathrm{W}$. When the contact load was $F_I = 4.0 \times 10^5 N$, the constrained resistance was obtained as R_{Ibc}=$6.86 \times 10^{-5}(°c \cdot m^2)/\mathrm{W}$. The ratio of both the constrained resistance and the bulk thermal resistance was 83% with the contact load of $4.0 \times 10^5 N$. The gap thermal resistance could be obtained as R_{Ig}=$2.98 \times 10^{-4}(°c \cdot m^2)/\mathrm{W}$, which accounted for 17% of the total TCR. Compared to the experimental result, the error of the proposed TCR model was approximately 9.8% . The results demonstrated that the proposed TCR model could accurately predict the TCR of annular contact surfaces with interference fits.

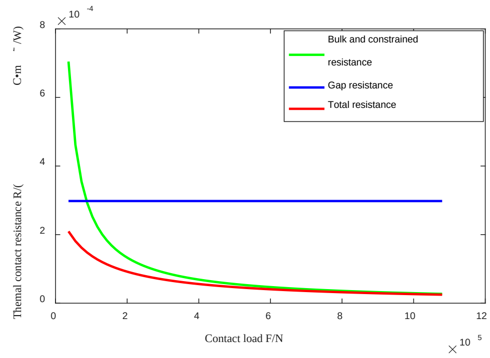

Fig. 9. Relationship between thermal contact resistance and contact load when $G = 1.0 \times 10^{-11}m$ and $D = 1.35$

Contact load determination of annular contact surface with transition and clearance fit

In addition to the interference fit, the transition and clearance fits for the test specimen also existed. The transition fit of the test specimen was $\Phi 80H6/k5$, where the nominal magnitude of the transition fit was $0.01\mathrm{mm}$. The clearance fit of the test specimen was $\Phi 80H6/g5$, where the nominal magnitude of the clearance fit was $-0.01\mathrm{mm}$. Similar to the interference fit, the radial distributions of the measured temperature for the transition and clearance fits of the two test specimens are presented in Fig. 10.

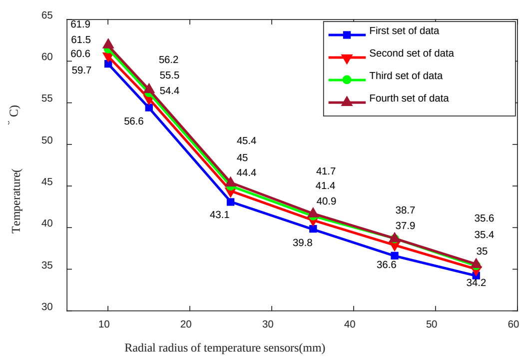

(a) transition fit ($\Phi 80H6/k5$)

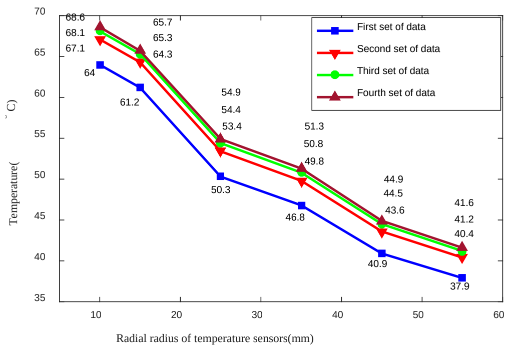

(b) clearance fit ($\Phi 80H6/g5$)

Fig. 10. Measured data of annular surfaces with transition and clearance fits

Similarly, by considering the average temperature from Fig. 10(a) and (b) in Eqs. (1), (2) and (3), the TCR of the annular contact surface with the transition and clearance fits could be obtained as $R_T^* = 1.2 \times 10^{-4} (°c \cdot m^2)/\mathrm{W}$ and $R_c^* = 1.4 \times 10^{-4} (°c \cdot m^2)/\mathrm{W}$, respectively. For the transition and clearance fits, it was difficult to theoretically obtain the TCR from the TCR model due to no contact. Therefore, only the effect of gap thermal resistance for the annular contact surface was considered. In fact, contact loads for transition and clearance fits existed and the TCR was not only the gap thermal resistance. As the proposed TCR model was reasonable, the experimental TCR values of the transition and clearance fits were added into the TCR model respectively. For the transition fit, the contact load was obtained as $F_T = 1.3 \times 10^5 N$, which was 32% of the interference fit. The bulk and constrained thermal resistance could be obtained as R_{Tbc}=$2.0 \times 10^{-4} (°c \cdot m^2)/\mathrm{W}$. The ratio of both the constrained thermal resistance and the bulk thermal resistance was 60%. The gap thermal resistance could be obtained as R_{Tg}=$2.97 \times 10^{-4} (°c \cdot m^2)/\mathrm{W}$, which accounted for 40% of the total TCR. For the clearance fit, the contact load was obtained as $F_C = 0.88 \times 10^5 N$, which was 22%of the interference fit. The bulk and constrained thermal resistance could be obtained asR_{Cbc}=$2.90 \times 10^{-4} (°c \cdot m^2)/\mathrm{W}$. The ratio of both the constrained thermal resistance and the bulk thermal resistance was 50%. The gap thermal resistance was obtained as R_{Cg}=$2.93 \times 10^{-4} (°c \cdot m^2)/\mathrm{W}$, which accounted for 50% of the total TCR. It could be observed that contact loads for the transition and clearance fits still existed, whereas the lower contact load, the higher gap thermal resistance ratio and the gap thermal resistance should not be ignored for a light contact load of the annular contact surfaces.

Discussion of surface profile effect on TCR

The thermal contact resistance of the annular contact surface was affected by the contact load F. Moreover, the surface profile was another main influencing factor for the thermal contact resistance of the annular contact surfaces, which could be depicted by the fractal dimension D and the fractal roughness parameter G. Fig.10 presents the relationship between thermal contact resistance and the fractal parameters under various contact loads. The thermal contact resistance decreased with the fractal dimension D improvement, whereas it decreased with the fractal roughness parameter G improvement, as presented in Fig.11 (a) and (b). The higher fractal dimension and the lower fractal roughness parameter represented a smoother contact surface. The thermal contact resistance decreased rapidly when the fractal dimension changed from 1.3 to 1.4 and increased when the fractal roughness parameter changed from$2.0 \times 10^{-12} m$ to $10 \times 10^{-12} m$. It could be observed that the annular contact surface improvement effectively decreased the thermal contact resistance.

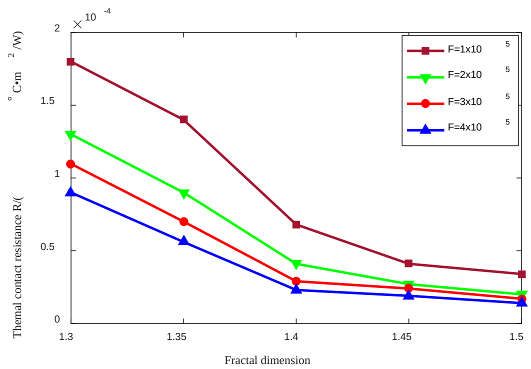

(a) $G = 1.0 \times 10^{-11} m$

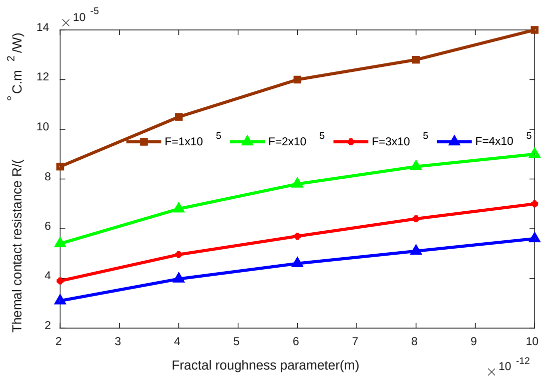

(b) $D = 1.35$

Fig. 11. Relationship between thermal contact resistance and fractal parameters under various contact loads

CONCLUSIONS

In this work, an experimental set-up with an annular interface was designed to obtain the TCR for various tolerance fits. A fractal theory based TCR model was proposed to predict the TCR of the annular contact surfaces with various tolerance fits for the spindle-bearing joint.

(1) For the interference fit, the error between the experimental data and the TCR model was 9.8%, which demonstrated that the proposed model could accurately predict the TCR of the annular contact surface.

(2) Contact loads for the transition and clearance fits still existed, whereas the lower contact load, the

higher gap thermal resistance ratio and the gap thermal resistance should not be ignored for a light contact load of the annular contact surfaces.

(3) The thermal contact resistance decreased with the fractal dimension D improvement, whereas it decreased with the fractal roughness parameter G improvement

ACKNOWLEDGMENT

This project was supported by National Natural Science Foundation (No. 51575009), Beijing Science and Technology Major Project (No. K2001011201801) and Scientific Research Plan of Beijing Municipal Education Commission (No. KM201710005016).

REFERENCES

Zhang, P., Xuan, Y.M. and Li, Q., A high-precision instrumentation of measuring thermal contact resistance using reversible heat flux[J]. Experimental Thermal & Fluid Science, Vol.54, pp.204-211(2014).

Zhang, P., Li, Q. and Xuan, Y.M., Thermal contact resistance of epoxy composites incorporated with nano-copper particles and the multi-walled carbon nanotubes[J]. Composites Part A Applied Science & Manufacturing, Vol.57, pp.1-7(2014).

Raza, K., Khalid, F.A., and Mabrouki, T., Numerical Investigation of the Effect of Interfacial Thermal Resistance upon the Thermal Conductivity of Copper/Diamond Composites[J]. Materials & Design, Vol.86 pp.248-258(2015).

Zheng, J., Li, Y. and Wang, L., An improved thermal contact resistance model for pressed contacts and its application analysis of bonded joints[J]. Cryogenics, Vol. 61, pp.133-142(2014).

Ahadia, M., Andisheh-Tadbira, M. and Tamb, M., An improved transient plane source method for measuring thermal conductivity of thin films: Deconvoluting thermal contact resistance[J]. International Journal of Heat & Mass Transfer, Vol.96 pp.371-380(2016).

Zhang, P., Cui, T.F. and Li, Q., Effect of surface roughness on thermal contact resistance of aluminium alloy. Applied Thermal Engineering, Vol. 121, pp.992–998(2017).

Majumdar, A. and Tien, C.L., Fractal characterization and simulation of rough surfaces. Wear, Vol.136, pp.313-327(1990).

Majumdar, A. and Bhushan, B. Fractal model of elastic-plastic contact between rough surfaces. ASME J Tribol, Vol.113, pp.1–11(1991).

Xu, M., Jiang, S.Y. and Cai, Y., An improved thermal model for machine tool bearings. International Journal of Machine Tools & Manufacture, Vol.47, pp.53-62(2007).

Zou, M., Yu, B. and Cai J., Fractal model for thermal contact conductance, Journal of Heat Transfer, Vol.130, pp.1013-1017(2008).

Chen, Y.P., Fu, P.P., and Zhang, C.B., Numerical simulation of laminar heat transfer in microchannels with rough surfaces characterized by fractal Cantor structures, International Journal of Heat and Fluid Flow, Vol.31, pp.622–629(2010).

Ji, C., Zhu, H., and Jiang, W., Fractal prediction model of thermal contact conductance of rough surfaces, Chinese Journal of Mechanical Engineering, Vol.26, pp.128-136(2013).

Jiang, S.Y., and Zhen, Y.J., An analytical model of thermal contact resistance based on the Weierstrass-Mandelbrot fractal function. Proceedings of the Institution of Mechanical Engineers, Part C: Journal of Mechanical Engineering Science, Vol.224, pp. 959–967(2010).

Fang, W.Z. and Gou, J.J., A multi-block lattice Boltzmann method for the thermal contact resistance at the interface of two solids. Applied Thermal Engineering, Vol.135, pp.122-132(2018).

Ma, C. and Zhao, L., A geometrical–mechanical–thermal predictive model for thermal contact conductance in vacuum environment. Proceedings of the Institution of Mechanical Engineers, Part B: Jounal of Engineering Manufacture, Vol.230, pp.1451-1464(2016).

Surya, K. and Andallib, T., Steady state experimental investigation of thermal contact conductance between curvilinear contacts using liquid crystal thermography. International Journal of Thermal Sciences, Vol. 118, pp.53-68(2017).

Vladislav, A. and Yastrebov., On the accurate computation of the true contact-area in mechanical contact of random rough surfaces. Tribology International Vol. 114, pp.161–171(2017).

Wang, C.C. and Lee, T.E., Nonlinear dynamic analysis of bi-directional porous aero-thrust bearing systems. Advances in Mechanical Engineering, Vol.12, pp.1-11(2017).

Wang, C.C. and Lee, R.M., Nonlinear analysis and simulation of active hybrid aerodynamic and aerostatic bearing system. Journal of Low Frequency Noise, Vibration and Active Control Vol. 3, pp.1404–1421(2019).

Shi, J.P., Cao, X.S., and Zhu, H., Tangential Contact Stiffness of Rough Cylindrical Faying Surfaces Based on the Fractal Theory. Journal of tribology–transactions of the ASME, Vol.136(2014).

Madhusudana, C.V., Thermal contact conductance[M]. New York: Springer-Verlag, 2014.

Jiang, S., Zheng, Y. and Zhu, H., A Contact Stiffness Model of Machined Plane Joint Based on Fractal Theory[J]. Journal of Tribology, Vol.132(2010)

Yovanovich, M.M., DeVaal, J.W. and Hegazy, A.A., A statistical model to predict thermal gap conductance between conforming rough surfaces[J]. AIAA paper, Vol. 82, pp.7-11(1982).

Song, S. and Yovanovich, M.M., Contact Interface Gas Heat Transfers: A Method of Measuring Thermal Accommodation Coefficient[C].9th Annual International Electronic Packaging Conference. Vol.2 pp. 925-936(1989).

Jian, S. and Dong, C., FEM Analysis of Stress on Shaft-Sleeve Interference Fits[J]. Aterials Science and Engineering II, Vol. 668, pp.495-499(2013).

Zhang, R.Z. and Cai, B.W. Numerical Method of the Power Spectral Density [J]. High Power Laser and Particle Beams, Vol. 12, pp.661~664(2000).

NOMENCLATURE

$R_{i,j}$ radius of the temperature sensors, mm

$T_{i,j}$ measured temperature, ℃

q_{R_X} heat flux, w/m^2

R TCR, $(°c \cdot m^2)$/w

f contact load for one micro-contact, N

a' truncated area of a micro-contact, μm^2

A_r real contact area, μm^2

r TCR of a micro-contact, $(°c \cdot m^2)$/w

Δ effective magnitude of interference, mm

p the contact stress, Mpa

D the fractal dimension

G fractal roughness parameter, m

F total normal load, N

a'_c critical area, μm^2

$u(r)$ displacement of the test specimen, mm

主軸-軸承不同公差配合下環形結合面接觸熱阻模型

方翠 楊聰彬 趙永勝 劉志峰
北京工業大學先進製造與智慧技術研究所

胡秋實
江蘇科技大學機械工程學院

摘 要

主軸-軸承結合面接觸熱阻是分析高速電主軸熱特性的關鍵，它會嚴重影響機床的加工精度。在本研究中，設計實驗裝置，通過實驗和一維穩態測量方法獲得不同公差配合下的環形接觸面的接觸熱阻。考慮壓縮熱阻、基體熱阻和間隙空氣熱阻建立不同公差配合下主軸-軸承環形結合面接觸熱阻模型。最後，將主軸-軸承間的間隙、過渡和過盈配合作為三種典型情況進行分析。對於過盈配合，根據所建立的模型可以計算其接觸熱阻，並根據接觸公式推導出接觸載荷。但該公式不適用於間隙配合和過渡配合,在這種情況下,採用混合方法來確定間隙配合和過渡配合的等效接觸載荷，並與實驗對比，結果表明，該模型可用於預測不同公差配合下環形接觸面的接觸熱阻。